Open Access

Catalysis Research

LIDSEN Publishing Inc.

Original Research

Removal of As(III) from Water by Cellulase Templated TiO_2: A Photocatalytic Oxidation Conjugated Adsorption Process

Liang Jiang, Lulu Xie, Jiao He *, Juanxue Kang, Wei Wang, Jiaqiang Wang *

School of Engineering, National Center for International Research on Photoelectric and Energy Materials, School of Materials and Energy, School of Chemical Sciences & Technology, Yunnan University, Kunming 650091, P.R. China; E-Mails: jqwang@ynu.edu.cn; 1693640694@qq.com; hejiao@ynu.edu.cn; 296177376@qq.com; wangwei2@ynu.edu.cn; jqwang@ynu.edu.cn

* **Correspondences:** Jiao He and Jiaqiang Wang; E-Mails: hejiao@ynu.edu.cn; jqwang@ynu.edu.cn

Academic Editor: Ermelinda Falletta

Special Issue: Recent Advances in TiO2 Photocatalysis and Applications

Catalysis Research
2022, volume 2, issue 3
doi:10.21926/cr.2203025

Received: July 16, 2022
Accepted: September 02, 2022
Published: September 09, 2022

Abstract

TiO_2 photocatalyst was prepared using cellulase as a biotemplate through a hydrothermal process. The as-prepared catalyst was characterized based on physicochemical techniques and was used to remove As(III) from contaminated water. The cellulase templated TiO_2 photocatalyst (TiO_2-cellulase) had a large specific surface area, which reached 166.6 $m^2 \cdot g^{-1}$. It also had a strong oxidation ability and, thus, behaved well in both photocatalytic oxidation of As(III) and dark adsorption. The pH of the solution had a negligible effect on the removal rate. TiO_2-cellulase had a higher photocatalytic removal rate of As(III) than commercial Degussa P25 TiO_2.

Keywords

As(III) removal; TiO_2; cellulase; biotemplate; photocatalysis

1. Introduction

Arsenic (As) contamination of water, and the resulting arsenic poisoning that seriously affects large groups of people, is an acute problem in many countries. The chronic toxicity of arsenic in drinking water can lead to various types of cancer, including liver, lung, kidney, bladder, and skin cancer, among others [1-3]. The removal of arsenic from solutions with high ionic strength is a major challenge for various water treatment technologies, including ion exchange, adsorption, reverse osmosis, and nanofiltration [4]. There are many techniques for the detection and adsorption of arsenic. For example, one study described the detection and adsorption of arsenic compounds through functional optical fibers, and the results showed that the proposed APTES-alginate-Ca^{+} system had As(V) selectivity. The adsorption of As(V) was due to the electronic stability in the molecular system and its binding energy [5]. Most changes in As adsorption are affected by the pH of the solution and the concentration of As [6]. Additionally, ion exchange and complexation strongly influence arsenic adsorption [7]. In native water, inorganic arsenic mainly exists in two oxidation states, As(V) and As(III). As(III) is more toxic than As(V); it has higher fluidity and lower affinity for the adsorbent [8]. The oxidation of As(III) species is ideal for enhancing arsenic immobilization. Therefore, common arsenic removal technologies include photocatalytic treatment of arsenide and the pre-processing of As(III) oxidation, followed by coprecipitation/adsorption of As(V) onto metal hydroxide [9]. For photocatalytic treatment, TiO_2 has been widely studied because of its non-toxicity and high photostability [10]. However, there are several methods to improve visible light absorption and the photocatalytic efficiency of TiO_2 nanoparticles, such as adding decorative metal nanoparticles, replacing non-metal atoms with metal atoms [11], and coupling with other semiconductors [12]. For As(III) oxidation treatment, chlorine compounds, ozone, H_2O_2, permanganate or manganese oxide, and Fenton reagent might be used as the oxidant for As(III) oxidation [13-20]. The photocatalytic oxidation of As(III) is an effective method. Among them, TiO_2 has been widely studied because of its non-toxicity and high photostability. For example, As(III) was oxidized to As(V) in the suspension of TiO_2 (Degussa P25) irradiated by ultraviolet light [21, 22]. To remove As(III) in one step, a prior oxidization step to convert As(III) to As(V) and the following adsorption of As(V) are essential for photocatalysts. However, Degussa P25 TiO_2 has a low capacity to adsorb arsenic. Generally, increasing the specific surface area of an adsorbent can increase its adsorption ability. Therefore, developing photocatalysts with a high specific surface area is an effective method to remove arsenic in water.

Biological templates have been investigated for the synthesis of porous inorganic materials, as they can derive morphologically controllable materials with structural specificity and unique functions [23-27]. In another study, we showed that the specific surface area of TiO_2/SiO_2 prepared by using diatoms as the biotemplate was significantly higher than the specific surface area of conventional TiO_2/SiO_2, which might be due to the formation of many accessible pores and channels [28]. Additionally, many biomolecules, such as peptides, proteins, enzymes, nucleic acids, or antibodies, may be captured in sol-gel matrices to build functional inorganic materials [29]. Based on the synthesis of biomolecular templates, nanomaterials, such as PbS quantum dots, were synthesized by luciferase, and CdS quantum dots were synthesized by the organophosphorus acid an hydrolase biological template [30, 31]. Additionally, an enzyme-mediated in-situ synthesis of Ag–TiO_2 using Escherichia coli as a biological template for dye degradation was proposed [32]. Enzymes are extremely effective in catalyzing various reactions under environmental and physiological

conditions. Thus, there is great interest in using enzymes as templates to synthesize inorganic nanomaterials.

Cellulase mainly consists of endoglucanase, exonuclease, and β-glucosidase [33] and is an active protein with catalytic power [34]. Among them, endoglucanase acts mainly on amorphous and crystalline regions and truncates long-chain cellulose molecules by random hydrolysis of β-1,4-glycoside bonds to produce small molecules of cellulose with reducing ends. Exodexranase hydrolyzes the β-1,4-glycosidic bond and acts on the end of the cellulose molecule, cutting one fibrodiosacrose molecule at a time. Glucosidase reduces the feedback inhibition reaction of some hydrolysates and breaks down fibrodiose glycose into glucose molecules [35-37]. Cellulase can catalyze the decomposition of cellulose and some related polysaccharides. The cellulose template substantially improves thermal stability and increases the surface area. A study reported the removal of CO_2^+ and Ni^{2+} in water by bagasse cellulose [38]. In this study, TiO_2-cellulase was prepared by using cellulase as a template under hydrothermal conditions. The TiO_2-cellulase combined the processes of photocatalytic oxidation and adsorption. Thus, it can oxidize As(III) to As(V), and also adsorb and remove As(V). It is a new strategy for removing As(III) and is different from the use of synergistic oxidant and adsorbent reported in other studies. Additionally, TiO_2-cellulase can oxidize and adsorb efficiently, and it performs the photocatalysis of As(III) more effectively than commercial Degussa P25 TiO_2.

2. Materials and Methods

2.1 Preparation of Cellulase Templated Mesoporous TiO_2 (TiO_2-cellulase)

Mesoporous TiO_2 samples were synthesized by a biomacromolecule templated hydrothermal process. Briefly, 1.0 g of cellulose from Trichoderma viride was dispersed in 30 mL of anhydrous ethyl alcohol by stirring for 30 min, and 3.0 g of TTIP was added. Then, 40 mL of distilled water was added dropwise with continued stirring. After stirring for 24 h, the mixture was transferred to a Teflon bottle and treated at 363 K under self-pressure for seven days without agitation. The mixture was filtered, and the final solid product was dried and calcinated at 673 K for 4 h. For comparison with P25 TiO_2, two photocatalysis reaction tubes were taken, and50 mL of the prepared As(III) solution was added. Next, 25 mg of TiO_2-cellulase was added to tube 1, and add 25 mg of P25 TiO_2 was added to tube 2. The samples were taken after dark reaction for 9 h, and the concentration of total As was measured. Then the samples were exposed to a UV lamp for 1 h, and measured the concentration of total As.

2.2 Characterization

Powder X-ray diffraction (XRD) experiments were conducted using a D/max-3B spectrometer with Cu Kα radiation, and scans were performed in the 2θ range of 10–90° with a scan rate of 10°/min (wide-angle diffraction). Using the Micromeritics Tristar II surface area and porosity analyzer, the distribution of the pore size, BET surface area, and pore volume were measured by nitrogen adsorption/desorption. Before conducting the analysis, the samples were degassed at 573 K for 3 h. With an acceleration voltage of 15 kV and a sample chamber pressure of 1 Torr, scanning electron microscopy (SEM) images were taken using a FEIQuanta200FEG microscope. High-resolution transmission electron microscopy (HRTEM) micrographs were obtained using a JEM-2100

microscope. FT-IR measurements were performed using a Thermo Nicolet 8700 instrument. Potassium bromide particles containing 0.5% catalyst were used in the FT-IR experiments and 32 scans were obtained for each transmission spectrum at a spectral resolution of 4 cm^{-1}. The dry KBr spectra were used for background subtraction. The UV-vis diffuse reflectance spectra (DRS) were measured (200–800 nm) in the air at room temperature using a Shimadzu UV-2401PC photometer.

2.3 Photocatalytic Activity

The reserved As(III) solution with a concentration of 1,000 mg/L was purchased from the National Analysis Center for Iron and Steel (NACIS, Beijing, China). In the experiment, the standard stock solution was diluted to 0.10 mg/L. Then, 2.5 mg of TiO_2-cellulase was added to 50 mL of the above-mentioned solution under agitation. A UV lamp (105 W; Tungsram, 360 nm) was used as the light source, which was located 15 cm above the reactor vessel. Before irradiation, the suspensions were magnetically stirred in the dark for about 9 h to ensure that an adsorption/desorption equilibrium was established. During specific irradiation intervals, 2 mL of the suspension was collected and filtered using a 0.45 μm microporous filter to remove the solid. The total arsenic concentration in the remaining solution was detected by a nondispersive atomic fluorescence spectrometer (AFS) (Pgeneral PF-6, Beijing). Speciation of As(III) and As(V) in the sample solution was detected by performing liquid chromatography-tandem mass spectrometry (LCMS) (Shimadzu LCMS-8030). The photocatalytic removal rate of arsenic was calculated using equation (1), where C_0 and C indicate the initial absorption and instantaneous absorption of As, respectively. The first-order rate constant k (min^{-1}) was calculated using equation (2), where C_e indicates the equilibrium adsorption of As and C indicates the instantaneous adsorption of As at time t.

$$Removal\ rate = \frac{C_0 - C}{C_0} \cdot 100\% \quad (1)$$

$$ln\frac{C_e}{C} = kt \quad (2)$$

3. Results and Discussion

3.1 Characterization of TiO_2-cellulase

In this study, TiO_2-cellulase was prepared by the hydrothermal method. The nanoparticles prepared using the hydrothermal method were highly crystalline and had larger surface areas than those prepared by the sol-gel method. The surface areas of the nanoparticles prepared by the hydrothermal and sol-gel methods were 18.2 $m^2 \cdot g^{-1}$ and 9.69 $m^2 \cdot g^{-1}$, respectively. This indicated that $CaTiO_3$ prepared by the hydrothermal method had higher photocatalytic activity [39]. The XRD pattern of the sample prepared using cellulase as the template is shown in Figure 1. The peaks of the 2θ values at 25.3°, 37.8°, 48.0°, 54.0°, 55.1°, 62.8°, 69.0°, 70.4°, 75.1°, and 82.9° corresponded to the (101), (004), (200), (105), (211), (204), (116), (220), (215), and (224) crystallographic planes of anatase TiO_2 (JCPDS, No. 84–1285), respectively. No peaks representing other phases were observed, indicating the formation of pure phases of anatase TiO_2.

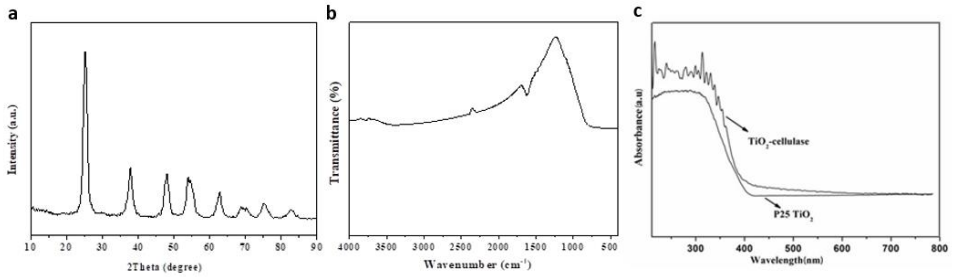

Figure 1 (a) The XRD pattern of TiO_2-cellulase. (b) The FT-IR spectrum of TiO_2-cellulase. (c) The UV-Vis diffuse reflectance spectra of TiO_2-cellulase and P25 TiO_2.

The bonding properties of the functional groups in TiO_2-cellulase were determined by performing FT-IR spectroscopy, as shown in Figure 1b. The band from 500 cm^{-1} to 590 cm^{-1} represents the Ti-O-Ti stretching vibration in TiO_2. The absorption peak at approximately 1,620 cm^{-1} was associated with the stretching and band-like vibrations of surface water molecules, including hydroxyl groups and molecular water, on the samples [40, 41]. No peaks corresponding to-CH,-CH_2, or-CH_3 bonds were observed, indicating that the C elements in the TiO_2 sample did not contain organic species from the cellulase template. After calcination at 673 K, organic species from cellulase were completely removed.

To determine the band gap, the UV-vis diffuse reflectance spectra of the as-prepared TiO_2-cellulase were measured. For comparison, the diffuse reflectance UV-Vis spectra of P25 TiO_2 and TiO_2-cellulase are shown in Figure 1c. TiO_2-cellulase showed absorption in the UV region and shifted the absorption edge of TiO_2 to the visible light range. In contrast, P25 TiO_2 did not show any considerable shift in the absorption spectra. The wavelength at the absorption edge (λ) is determined as the intercept on the wavelength axis for a tangent line drawn on the absorption spectra. By applying this method, the absorption edge for TiO_2-cellulase was found to be 400 nm, corresponding to a band gap of 3.1 eV, which was lower than the band gap of P25 TiO_2. This showed that TiO_2-cellulase has a stronger light absorption ability than P25 TiO_2, which can enhance the utilization of photons and increase the production of photoexcited electron/hole pairs, thus improving the photocatalytic performance of TiO_2-cellulase.

The N_2 adsorption/desorption isotherms for TiO_2-cellulase and the corresponding pore size distribution are shown in Figure 2. The isotherms were classified as type IV with hysteresis, which is the characteristic of mesoporous materials. The isotherm of the TiO_2-cellulase sample was type IV with an H3-type hysteresis loop, associated with mesopores present in aggregates composed of primary particles, giving rise to pileup pores. The pore size distribution consisted of a single narrow peak. The Brunauer-Emmett-Teller (BET) surface area, pore volume, and average pore diameter for TiO_2-cellulase were 166.6 $m^2 \cdot g^{-1}$, 0.26 $cm^3 \cdot g^{-1}$, and 5.0 nm, respectively. Thus, the biotemplated process greatly influenced the BET surface area of the samples.

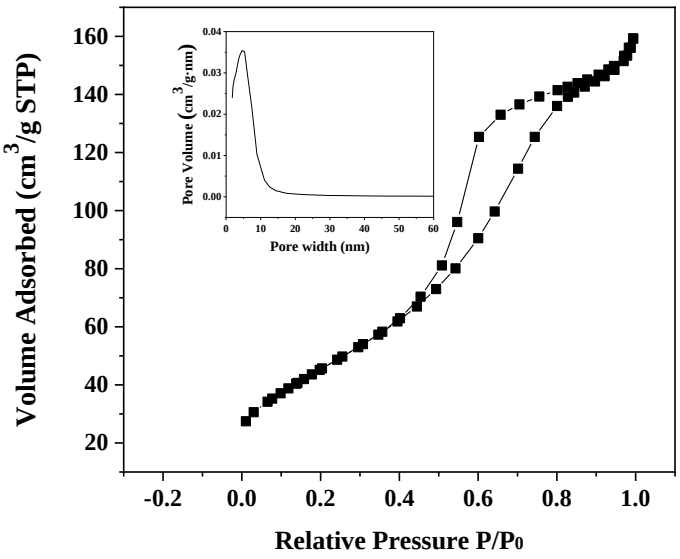

Figure 2 The N_2 adsorption/desorption isotherms and the pore size distribution curves (inset) of TiO_2-cellulase.

The SEM and TEM images showed that the TiO_2-cellulase nanomaterial consisted of an assemblage of dense nanoparticles (Figure 3). The HRTEM image of an enlarged rectangle area in Figure 3c shows lattice spacing of 0.35 nm, matching that of the (101) plane of anatase TiO_2.

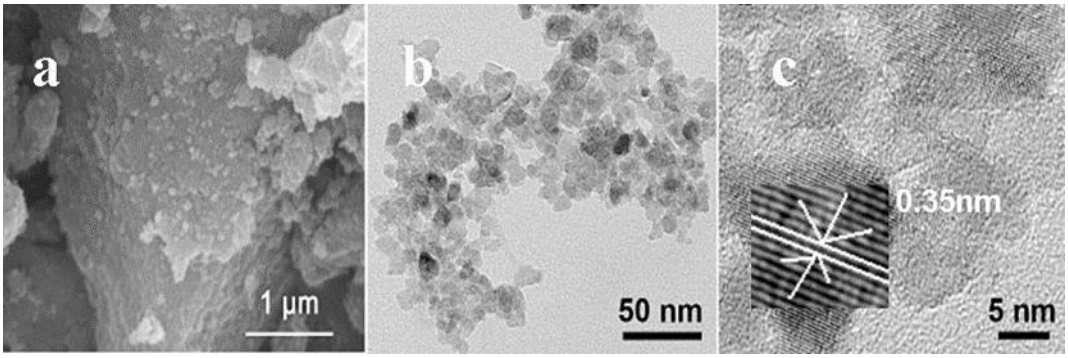

Figure 3 The (a) SEM, (b) TEM, and (c) HRTEM images of TiO_2-cellulase.

3.2 Removal of As(III) over TiO_2-cellulase

3.2.1 Catalyst Amount Effect

The amount of TiO_2-cellulase ranged from 0 mg to 50 mg at a constant initial arsenic concentration of 1.0 mg/L after exposure to UV light for 6 h. The total arsenic concentration decreased with an increase in the amount of TiO_2-cellulase (Figure 4). When the amount of TiO_2-cellulase reached 2.5 mg, the total arsenic concentration decreased to 0.01 mg/L. Further increase in the amount of TiO_2-cellulase showed a negligible change in the total arsenic concentration. Thus, the optimal amount of TiO_2-cellulase was selected as 2.5 mg.

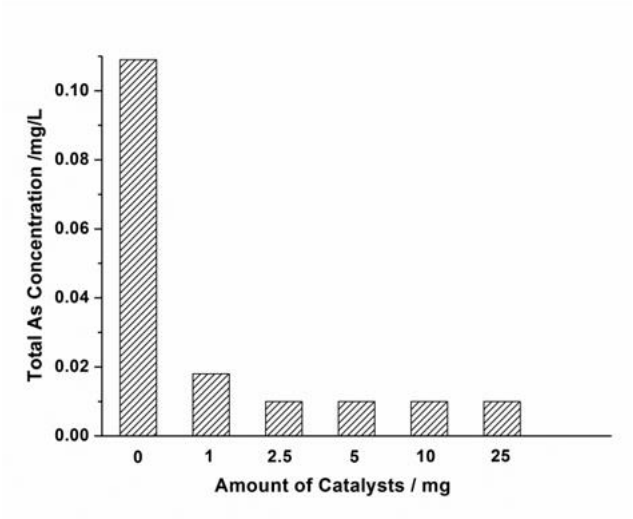

Figure 4 The effect of the amount of catalyst on the total As concentration.

3.2.2 Reaction Time Effect

The change in the total arsenic concentration during the irradiation of UV light in the presence of 2.5 mg TiO_2-cellulase was recorded. The results showed that the total arsenic concentration reached equilibrium after 1 h (Figure 5). The activity of the concentration of total As within 1 h with a removal rate of 81% in irradiated TiO_2-cellulase dispersions was determined, and only 40% of arsenic was adsorbed in the dark. This result suggested that UV light might improve the removal of arsenic in the presence of TiO_2-cellulase. In contrast, the photocatalytic removal rate of arsenic was only 56.8% for P25 TiO_2 under the same condition. Thus, TiO_2-cellulase showed higher removal efficiency than P25 TiO_2, which might be due to its larger surface area.

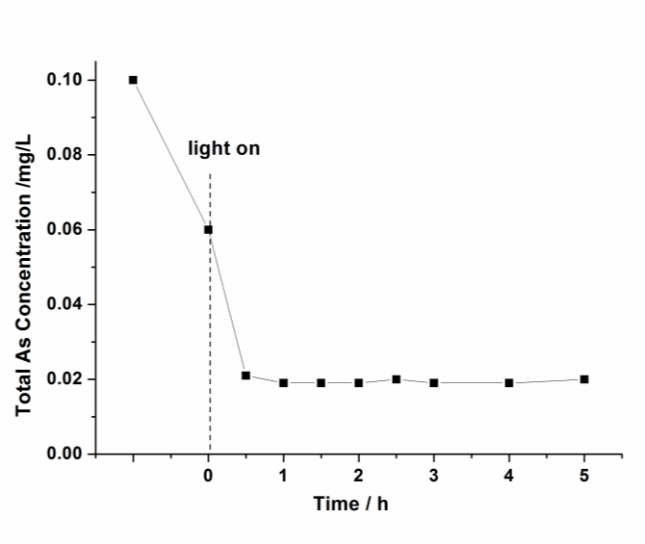

Figure 5 The effect of reaction time on the total As concentration in aqueous dispersions (catalysts = 2.5 mg).

3.2.3 Effect of pH

The effect of pH on the removal of arsenic in the dark and under irradiation is shown in Figure 6.

The removal rate of arsenic increased slightly from pH 2 to 9 in the dark and did not change after that, with an increase in the pH in irradiated TiO_2-cellulase dispersions. This occurred probably because the characteristics of the TiO_2 photocatalyst can remain stable over a wide range of pH [42], indicating that pH has a negligible effect on the removal of arsenic. The results suggested wide applicability of TiO_2-cellulase.

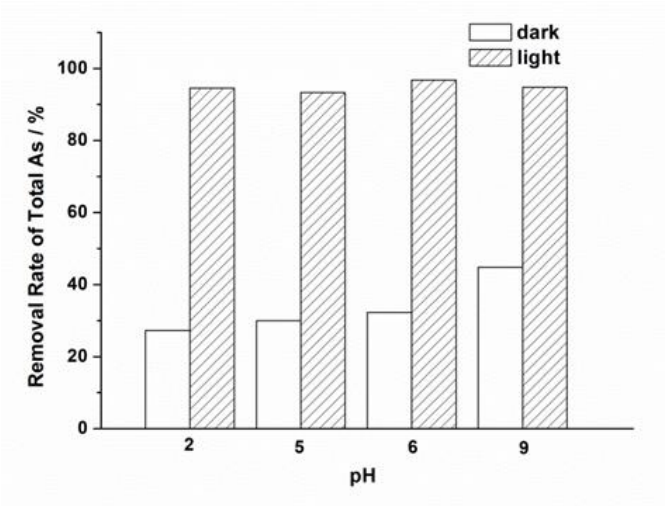

Figure 6 Effect of pH on total As concentrations in aqueous dispersions (catalysts = 2.5 mg).

3.2.4 Variation in the Valence and Concentration

The variation in the concentration of As(III) and As(V) under visible light is shown in Figure 7, which indicated the importance of light irradiation in the removal process. The concentrations of As(III) and As(V) reached 92 μg/L and 0 μg/L, respectively, in the dark in the presence of TiO_2-cellulase. Thus, As(III) was not oxidized in the dark. When the TiO_2-cellulase dispersions were exposed to UV light, the concentration of As(III) decreased, and that of As(V) increased within 25 min. After 30 min, the As(V) concentration also decreased. These results indicated that As(III) was oxidized to As(V) under light, and TiO_2-cellulase adsorbed As(V). This occurred because the semiconductor responsible for forming oxidant radicals is activated by UV light. The mechanism is as follows [43]:

$$① \ TiO_2 + h\nu \longrightarrow TiO_2(e^- + h^+)$$

$$② \ OH^- + h^+ \longrightarrow OH^{\cdot}$$

$$③ \ O_2 + e^- \longrightarrow O_2^{\cdot -}$$

$$④ \ As(III) + OH^{\cdot} \longrightarrow As(IV) + OH^-$$

$$⑤ \ As(III) + O_2^{\cdot -} + 2H^+ \longrightarrow As(V) + H_2O_2$$

$$⑥ \ As(IV) + O_2 \longrightarrow As(V) + O_2^{\cdot -}$$

$$⑦ \ O_2^{\cdot -} + e^- + 2H^+ \longrightarrow H_2O_2$$

$$⑧\ O_2^{\cdot-} + O_2^{\cdot-} + 2H^+ \longrightarrow H_2O_2 + O_2$$

$$⑨\ As(III) + H_2O_2 \longrightarrow As(V) + 2OH^-$$

$$⑩\ As(III) + h^+ \longrightarrow As(IV) + O_2 \longrightarrow As(V) + O_2^{\cdot-}$$

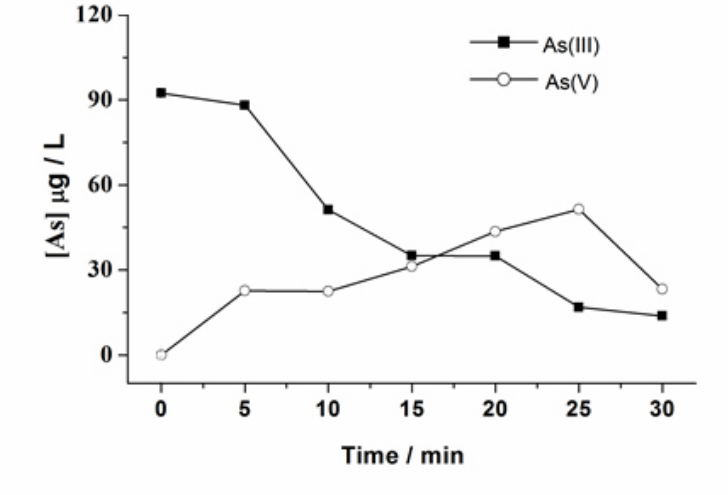

Figure 7 Changes in the concentration of As(III) and As(V) under visible light.

3.3 Comparison of the Removal Efficiency of As (III) between TiO_2-cellulase and P25 TiO_2

The concentration of total As was measured, and the results are shown in Table 1.

Table 1 Comparison of TiO_2-cellulase and P25 TiO_2 for the removal efficiency.

Material	Initial concentration (mg/L)	Concentration after dark reaction (mg/L)	Concentration after light reaction (mg/L)	Removal rate (%)
P25 TiO_2	0.088	0.038	0.028	56.8
TiO_2-cellulase	0.088	0.060	0.004	94.5%

The adsorption effect of P25 TiO_2 on As(III) in the dark reaction was better than that of TiO_2-cellulase, but the removal rate of As(III) by TiO_2-cellulase was significantly higher than that of P25 TiO_2 after light reaction adsorption (Table 1). The As(III) solution with an initial concentration of 0.088 mg/L was reduced to 0.004 mg/L after adding TiO_2-cellulase, which was within the latest standard of 0.01 mg/L used in many countries.

4. Conclusions

To summarize, cellulase was successfully used as a template to synthesize TiO_2 structures with anatase phases under hydrothermal conditions, which substantially improved the thermal stability and increased the surface area. The TiO_2-cellulase effectively performed the photocatalysis of As(III), and the performance was considerably better than that of commercial Degussa P25 TiO_2.

When the amount of TiO_2-cellulase reached 2.5 mg, the highest photocatalytic removal rate of 81% was achieved under UV light irradiation. The high removal rate of total arsenic facilitated by TiO_2-cellulase at different values of pH suggested its wide applicability, and we suggest that the synthetic strategy presented here might be extended to other mesoporous materials. The TiO_2-cellulase photocatalyst might also be able to effectively purify water contaminated with toxic ions, such as those of arsenic and other heavy metal elements.

Acknowledgments

The authors thank the National Natural Science Foundation of China (22062026). The authors also thank The Yunling Scholar (K264202012420), the Industrialization Cultivation Project (2016CYH04), the Basic Research Projects of Yunnan Province (202101AT070017), the Key Projects for Research and Development of Yunnan Province (2018BA065), the Key Laboratory of Advanced Materials for Wastewater Treatment of Kunming for financial support, the authors also thank the Advanced Analysis and Measurement Center of Yunnan University for the sample testing service.

Author Contributions

Jiaqiang Wang conceived and designed the experiments; Lulu Xie performed the experiments; Jiao He and Juanxue Kang analyzed the data; Wei Wang contributed reagents/materials/analysis tools; Liang Jiang wrote the paper.

Competing Interests

The authors declare no conflict of interest.

References

1. Brown KG, Boyle KE, Chen CW, Gibb HJ. A dose-response analysis of skin cancer from inorganic arsenic in drinking water[1]. Risk Anal. 1989; 9: 519-528.
2. Smith AH, Hopenhayn-Rich C, Bates MN, Goeden HM, Hertz-Picciotto I, Duggan HM, et al. Cancer risks from arsenic in drinking water. Environ Health Perspect. 1992; 97: 259-267.
3. Huq ME, Fahad S, Shao Z, Sarven MS, Al-Huqail AA, Siddiqui MH, et al. High arsenic contamination and presence of other trace metals in drinking water of Kushtia district, Bangladesh. J Environ Manage. 2019; 242: 199-209.
4. MacPhee MJ, Charles GE, Cornwell DA, Sorg TJ. Treatment of arsenic residuals from drinking water removal processes. Washington, DC: US Environmental Protection Agency, National Risk Management Research Laboratory, Office of Research and Development; 2001; EPA/600/R-01/033.
5. Jauregui-Vazquez D, Aguilera-Granja F, Díaz-Cervantes E. Adsorption of arsenide through functionalized optical fiber: A finite model in silico approach as a perspective for sensing application. Chem Zvesti. 2022; 76: 2259-2266.
6. Chen Z, Kim KW, Zhu YG, Liu F, He JZ. Adsorption ($As^{III,V}$) and oxidation (As^{III}) of arsenic by pedogenic Fe–Mn nodules. Geoderma. 2006; 136: 566-572.
7. Zou SW, Koh KY, Chen ZH, Wang YY, Chen JP, Zheng YM. Adsorption of organic and inorganic arsenic from aqueous solution: Optimization, characterization and performance of Fe–Mn–Zr

ternary magnetic sorbent. Chemosphere. 2022; 288: 132634.
8. Wang L, Condit WE, Chen AS, Sorg TJ. Technology selection and system design US EPA arsenic removal technology demonstration program round[1]. Washington, DC: National Risk Management Research Laboratory, Office of Research and Development, US Environmental Protection Agency; 2004; EPA/600/R-05/001.
9. Bidone E, Cesar R, Santos MC, Sierpe R, Silva-Filho EV, Kutter V, et al. Mass balance of arsenic fluxes in rivers impacted by gold mining activities in Paracatu (Minas Gerais State, Brazil). Environ Sci Pollut Res. 2018; 25: 9085-9100.
10. Aguilera-Granja F, Aguilera–del–Toro RH, Vogel EE, Cisternas E. Bimetalic $(AuPt)_4$ nano-clusters adsorbed on TiO_2 nano-wires: A density-functional-theoretic study. J Phys Chem Solids. 2021; 159: 110275.
11. Aguilera–del–Toro RH, Aguilera-Granja F, Vogel EE. Structural and electronic properties of $(TiO_2)_{10}$ clusters with impurities: A density functional theory investigation. J Phys Chem Solids. 2019; 135: 109107.
12. Qiu J, Feng Y, Zhang X, Zhang X, Jia M, Yao J. Facile stir-dried preparation of gC_3N_4/TiO_2 homogeneous composites with enhanced photocatalytic activity. RSC Adv. 2017; 7: 10668-10674.
13. Hering JG, Chen PY, Wilkie JA, Elimelech M, Liang S. Arsenic removal by ferric chloride. J Am Water Work Assoc. 1996; 88: 155-167.
14. Oscarson D, Huang P, Liaw W, Hammer U. Kinetics of oxidation of arsenite by various manganese dioxides. Soil Sci Soc Am J. 1983; 47: 644-648.
15. Driehaus W, Seith R, Jekel M. Oxidation of arsenate (III) with manganese oxides in water treatment. Water Res. 1995; 29: 297-305.
16. Borho M, Wilderer P. Optimized removal of arsenate (III) by adaptation of oxidation and precipitation processes to the filtration step. Water Sci Technol. 1996; 34: 25-31.
17. Pettine M, Campanella L, Millero FJ. Arsenite oxidation by H_2O_2 in aqueous solutions. Geochim Cosmochim Acta. 1999; 63: 2727-2735.
18. Chiu VQ, Hering JG. Arsenic adsorption and oxidation at manganite surfaces. 1. Method for simultaneous determination of adsorbed and dissolved arsenic species. Environ Sci Technol. 2000; 34: 2029-2034.
19. Kim MJ, Nriagu J. Oxidation of arsenite in groundwater using ozone and oxygen. Sci Total Environ. 2000; 247: 71-79.
20. Dodd MC, Vu ND, Ammann A, Le VC, Kissner R, Pham HV, et al. Kinetics and mechanistic aspects of As(III) oxidation by aqueous chlorine, chloramines, and ozone: Relevance to drinking water treatment. Environ Sci Technol. 2006; 40: 3285-3292.
21. Comninellis C, Kapalka A, Malato S, Parsons SA, Poulios I, Mantzavinos D. Advanced oxidation processes for water treatment: Advances and trends for R&D. J Chem Technol Biotechnol. 2008; 83: 769-776.
22. Yang H, Lin WY, Rajeshwar K. Homogeneous and heterogeneous photocatalytic reactions involving As(III) and As(V) species in aqueous media. J Photochem Photobiol A. 1999; 123: 137-143.
23. Lee H, Choi W. Photocatalytic oxidation of arsenite in TiO_2 suspension: Kinetics and mechanisms. Environ Sci Technol. 2002; 36: 3872-3878.
24. Shakoor MB, Niazi NK, Bibi I, Shahid M, Sharif F, Bashir S, et al. Arsenic removal by natural and

chemically modified water melon rind in aqueous solutions and groundwater. Sci Total Environ. 2018; 645: 1444-1455.
25. Dhanasekaran P, Satya Sai PM, Anand Babu C, Krishna Prabhu R, Rajan KK. Arsenic removal from groundwater by Anjili tree sawdust impregnated with ferric hydroxide and activated alumina. Water Sci Technol Water Supply. 2016; 16: 115-127.
26. García-Rosales G, Longoria-Gándara LC, Cruz-Cruz GJ, Olayo-González MG, Mejía-Cuero R, Pérez PÁ. Fe-TiO_x nanoparticles on pineapple peel: Synthesis, characterization and As(V) sorption. Environ Nanotechnol Monit Manag. 2018; 9: 112-121.
27. Mao MQ, Wang JQ, He J, Yan ZY. Mesoporous materials catalysts for photodegradation of water pollutants: From chemical templates to biotemplates. In: New and future developments in catalysis. Amsterdam: Elsevier; 2013. pp. 443-469.
28. He J, Chen DM, Li YL, Shao JL, Xie J, Sun YJ, et al. Diatom-templated TiO_2 with enhanced photocatalytic activity: Biomimetics of photonic crystals. Appl Phys A. 2013; 113: 327-332.
29. Dickerson MB, Sandhage KH, Naik RR. Protein-and peptide-directed syntheses of inorganic materials. Chem Rev. 2008; 108: 4935-4978.
30. Ma N, Marshall AF, Rao J. Near-infrared light emitting luciferase via biomineralization. J Am Chem Soc. 2010; 132: 6884-6885.
31. Zhao L, Gattás-Asfura KM, Xu J, Patel RA, Dadlani A, Sillero-Mahinay M, et al. Organophosphorus acid anhydrolase bio-template for the synthesis of CdS quantum dots. Chem Commun. 2011; 47: 7242-7244.
32. Gunasekar V, Divya B, Brinda K, Vijaykrishnan J, Ponnusami V, Rajan KS. Enzyme mediated synthesis of Ag-TiO_2 photocatalyst for visible light degradation of reactive dye from aqueous solution. J Solgel Sci Technol. 2013; 68: 60-66.
33. Wang J, Hao X, Wen P, Zhang T, Zhang J. Adsorption and desorption of cellulase on/from lignin pretreated by dilute acid with different severities. Ind Crops Prod. 2020; 148: 112309.
34. Zhang Z, Wang X, Gao M, Yan H, Qiu L. Adsorption of cellulases on pulp fibers during pretreatment for microfibrillated cellulose film preparation. J Mater Sci. 2021; 56: 19267-19282.
35. Cai C, Jin Y, Pang Y, Ke Q, Qiu W, Qiu X, et al. Tracing cellulase components in hydrolyzate during the enzymatic hydrolysis of corncob residue and its analysis. Bioresour Technol Rep. 2018; 4: 137-144.
36. Liu XY, Jiang Y, Wang LJ, Song XP, Qin CR, Wang SF. Tuning of size and properties of cellulose nanofibers isolated from sugarcane bagasse by endoglucanase-assisted mechanical grinding. Ind Crops Prod. 2020; 146: 112201.
37. Xue D, Lin D, Gong C, Peng C, Yao S. Expression of a bifunctional cellulase with exoglucanase and endoglu-canase activities to enhance the hydrolysis ability of cellu-lase from a marine Aspergillus niger. Process Biochem. 2017; 52: 115-122.
38. Elias MM, Ferreira GM, de Almeida FT, Rosa NC, Silva IA, Filgueiras JG, et al. Synthesis and application of sugarcane bagasse cellulose mixed esters. Part I: Removal of Co^{2+} and Ni^{2+} from single spiked aqueous solutions in batch mode using sugarcane bagasse cellulose succinate phthalate. J Colloid Interface Sci. 2019; 533: 678-691.
39. Han C, Liu JJ, Yang WJ, Wu QQ, Yang H, Xue XX. Photocatalytic activity of $CaTiO_3$ synthesized by solid state, sol–gel and hydrothermal methods. J Solgel Sci Technol. 2017; 81: 806-813.
40. Lu MD, Yang SM. Synthesis of poly (3-hexylthiophene) grafted TiO_2 nanotube composite. J Colloid Interface Sci. 2009; 333: 128-134.

41. Sabzi M, Mirabedini S, Zohuriaan-Mehr J, Atai M. Surface modification of TiO_2 nano-particles with silane coupling agent and investigation of its effect on the properties of polyurethane composite coating. Prog Org Coat. 2009; 65: 222-228.
42. Nogueira RF, Jardim WF. Heterogeneous photocatalysis and its environmental applications. Quim Nova. 1998; 21: 69-72.
43. Ryu J, Choi W. Effects of TiO_2 surface modifications on photocatalytic oxidation of arsenite: The role of superoxides. Environ Sci Technol. 2004; 38: 2928-2933.